JOURNAL OF AIRCRAFT
Vol. 42, No. 2, March–April 2005

Aeroelastic System Development Using Proper Orthogonal Decomposition and Volterra Theory

David J. Lucia* and Philip S. Beran†
U.S. Air Force Research Laboratory, Wright–Patterson Air Force Base, Ohio 45433-7542
and
Walter A. Silva‡
NASA Langley Research Center, Hampton, Virginia 23681-0001

Volterra theory and proper orthogonal decomposition are combined into a hybrid methodology for reduced-order modeling of aeroelastic systems. The outcome of the method is a set of linear ordinary differential equations describing the modal amplitudes associated with both the structural modes and the proper orthogonal decomposition basis functions for the fluid. The structural modes are sine waves of varying frequency, and the new approach is applied to the fluid dynamics equations. The structural modes are treated as forcing terms that are impulsed as part of the fluid model realization. By the use of this approach, structural and fluid operators are coupled into a single aeroelastic operator while the parameter (or parameters) of interest for sensitivity analysis are preserved. The approach is applied to an elastic panel in supersonic crossflow. The resulting aeroelastic model provides correct limit-cycle oscillation prediction over a wide range of panel dynamic pressure values. Time integration of the reduced-order aeroelastic model is four orders of magnitude faster than the high-order solution procedure developed by the use of traditional fluid and structural solvers.

Nomenclature

A, B, C	=	state-space matrix operators
$\boldsymbol{a}$	=	panel deflection modal amplitudes a_i
$\boldsymbol{b}$	=	panel deflection speed modal amplitudes b_i
D	=	plate stiffness, $E_s h^3/12(1-\nu^2)$
D, P, Q	=	singular value decomposition products
$\boldsymbol{E}, \boldsymbol{F}$	=	vectors of X-axis and Y-axis fluxes
E_s	=	Young's modulus
E_T	=	total energy, $E_{Td}/\rho_\infty u_\infty^2$
H_{rs}	=	generalized Hankel matrix
h	=	panel thickness
$\boldsymbol{h}$	=	Volterra kernel function
K	=	number of time samples in impulse
L	=	reference length
M	=	Mach number
m_x, m_y	=	fluid momentum components, ρu and ρv
n	=	time index
$\boldsymbol{P}$	=	array of pressure differentials P_i on panel
p	=	pressure, $P_d/\rho_\infty u_\infty^2$
q	=	number of states in realization
R	=	flux calculation from the Euler equations
$\hat{R}$	=	reduced-order aeroelastic operator
r	=	size of shift in data window
S	=	matrix of flowfield data or snapshots
s	=	number of time samples in window, panel deflection speed, $\dot{w}$
t	=	time, $t_d u_\infty/L$
$\boldsymbol{U}, \hat{\boldsymbol{U}}$	=	full- and reduced-order discrete flow variables
$\boldsymbol{u}$	=	vector of forcing inputs
u, v	=	fluid velocity components, u_d/u_∞, and v_d/u_∞
V	=	matrix of eigenvectors of $S^T S$
w	=	normal panel deflection, w_d/L
$\boldsymbol{X}$	=	vector of dynamic states
x, y	=	spatial coordinates, x_d/L and y_d/L
$\boldsymbol{Y}$	=	vector of measurement data
$\boldsymbol{Y_m}$	=	Markov parameter
$\boldsymbol{Y_s}$	=	structural state array, $[\boldsymbol{b}, \boldsymbol{a}]^T$
α	=	expression containing structural parameters
β	=	scaling parameter
γ	=	ratio of specific heats
Δt	=	time-step size for integration
λ	=	nondimensional dynamic pressure, $\rho_\infty L/\rho_s h$
μ	=	mass ratio $\rho_\infty u_\infty^2 L^3/D$
ν	=	Poisson's ratio 0.3
ρ	=	fluid density, ρ_d/ρ_∞
ρ_s	=	structural density
Φ	=	proper orthagonal decomposition reduced-order mapping matrix

Subscripts

ae	=	aeroelastic quantity
d	=	dimensional quantity
f	=	fluid system
s	=	structural system
0	=	base flow
∞	=	freestream quantity

Introduction

THE application of reduced-order modeling (ROM) techniques to aeroelastic systems is an active area of research, motivated by the desire for faster algorithms that are well-suited to the design environment for aircraft. For example, transonic, fluid–structure interaction is a particular application of interest to both external and internal aerodynamicists because moving shock waves in the flow necessitate high-fidelity numerical flow solvers that are too cumbersome for iterative design analysis. Regardless of the application, when nonlinearities are present in either the flowfield or the structure, established order-reduction methods that rely on linearized dynamics are of little use.

Presented as Paper 2003-1922 at the AIAA/ASME/ASCE/AHS 44th Structures, Structural Dynamics, and Materials Conference, Norfolk, VA, 7 April 2003; received 30 April 2003; revision received 5 January 2004; accepted for publication 5 January 2004.

*Senior Research Aerospace Engineer, AFRL/VAS, Building 45, 2130 Eighth Street, Suite 1; david.lucia@wpafb.af.mil. Member AIAA.
†Principal Research Aerospace Engineer, AFRL/VASD, Building 146, 2210 Eighth Street; philip.beran@wpafb.af.mil. Associate Fellow AIAA.
‡Senior Research Scientist, Aeroelasticity Branch, Mail Stop 340. Senior Member AIAA.

Volterra methods[1] and proper orthogonal decomposition[2,3] (POD) are two of the more prevalent ROM techniques well-suited to nonlinear dynamics.[4–8] Traditionally, Volterra methods have relied on generalized aerodynamic forces (GAFs) to couple fluid forcing terms to structural modes. The combining of POD with Volterra methods is a way to replace the GAF terms with a physics-based fluid ROM that can potentially produce nonlinear aerodynamic forcing. Over the past three years, applications of POD to the Euler equations have produced reduced-order aeroelastic models that properly capture aerodynamic nonlinearities. A low-order POD representation of the discrete, two-dimensional Euler equations[9] was coupled with the von Kármán equation to simulate the dynamics of flow over a flexible panel.[10] Subsequently, a new approach was taken, involving domain decomposition, that allowed limit-cycle oscillations (LCO) to be simulated accurately in the transonic regime.[11] In that study, full- and reduced-order models of a small flow region containing a moving shock were decomposed from the larger flow domain. Both approaches enabled a physically consistent treatment of the aerodynamic nonlinearity. In a more recent paper,[12] the original POD/ROM methodology used for flow over an elastic panel[10] was revisited to improve the temporal coupling between the aerodynamic and structural dynamic equations. Furthermore, a modal representation of the structure was employed that permitted a more efficient formulation of the reduced-order aeroelastic system.

All of the studies just mentioned relied on a ROM technique called subspace projection for time integration of the reduced-order model. Although sufficient to demonstrate the accuracy of the POD basis functions, subspace projection was not an efficient way to time integrate the low-order, aeroelastic ROM. Generally, four orders of magnitude reduction in fluid system degrees of freedom (DOF) were demonstrated in the aforementioned studies. Time integrating these POD/ROMs with subspace projection generally produced about one order of magnitude improvement in compute time to accompany a much larger drop in problem order.

The applicability of POD basis functions to nonlinear problems has been documented in the literature, but a tractable nonlinear, low-order model realization procedure is a key missing link. Two techniques, Galerkin projection and direct projection, have been recently reported as having potential for obtaining nonlinear terms for POD/ROMs (see Ref. 13). However, the linear portion of these realization procedures is generally unstable, requiring dissipation techniques that affect model performance. The Volterra–POD approach provides a stable reduced-order equation set and is an important advance toward achieving stable, nonlinear reduced-order models.

The hybrid Volterra–POD method was recently developed for time integration of POD/ROMs applied to compressible flowfields.[14] The goal of the Volterra–POD approach was to achieve computational savings on the order of DOF reductions. This goal was achieved in the initial application, where four orders of magnitude reduction was obtained in both DOF and compute time. To date, the hybrid Volterra–POD method has been applied only to subsonic flowfields characterized by linear behavior with fixed boundaries. The product of the technique was a linear, state-space system of ordinary differential equations (ODEs) governing the dynamics of modal coefficients corresponding to a small number of POD basis functions. The state-space realization was obtained from a set of impulse responses that were processed using the eigensystem realization algorithm (ERA).[15,16]

This research will extend the Volterra–POD approach to supersonic flowfields with dynamic boundary behavior. The POD-Volterra method will be applied to a two-dimensional elastic panel in inviscid, supersonic crossflow. This aereolastic system exhibits LCO when the panel dynamic pressure is above a critical value. The Volterra–POD approach will be used to identify a low-dimensional, linear POD/ROM for the fluid. The POD/ROM will be tightly coupled to a low-dimensional, nonlinear model of the von Kármán plate equation (see Ref. 17). The aeroelastic response will be obtained by the use of an implicit time-integration scheme.

The Volterra–POD technique involves procedures that require the selection of parameters such as impulse size, several data windowing lengths, and impulse sampling frequency. The choice of POD basis affects performance as well. Some considerations for generation of the POD basis include choice of base flow (perturbation determined by POD/ROM to this base flow), snapshot collection method, and sampling frequency. (The method of snapshots[18] will be discussed in the next section.)

The research will consider two base flow cases and two snapshot collection methods. Both uniform flow at freestream conditions and steady-state flow over a static panel deflection will be considered as base flow cases. An aeroelastic POD basis will be generated by sampling a small portion of the time history for a baseline LCO case, which was the approach in recent applications by the use of subspace projection for this problem.[12] In addition, we will investigate use of the impulse response of the fluid system to generate a POD basis. The full-system impulse response is collected as part of the Volterra–POD approach, and the impulse responses can be sampled as snapshots in lieu of the LCO time history. Finally, we will apply POD to the structural dynamics, couple the structural POD/ROM with the fluid POD/ROM, and examine performance. We will record the various parameter settings used to generate the aeroelastic POD/ROMs for each case.

The linearity of the supersonic flowfield will be examined as part of the ROM analysis. The principle of superposition applies in a linear flowfield, which enables a host of linear order-reduction techniques, including the Volterra–POD technique detailed in this paper. Although the supersonic, aeroelastic flowfield is well represented by a linear fluid model, we will demonstrate that the supersonic flow-field itself is not linear in general.

The performance of the Volterra–POD aeroelastic ROMs will be quantified in accuracy, order reduction, and computational savings. A high-order, full-system representation of the problem is required for snapshot collection. The flowfield and panel response for the full-system model will serve as the baseline for performance comparison. Accuracy will be quantified by comparison of LCO panel response, flowfield pressure distribution on the elastic panel, LCO frequency, and LCO phase for a variety of panel dynamic pressure values. Finally, the robustness of the Volterra–POD method for the prediction of LCO response across a broad parameter space will also be addressed.

Model Problem Formulation

This section describes the full-system aeroelastic model for two-dimensional flow over a semi-infinite, pinned panel of length L.

Structural Dynamics Equations

Panel dynamics are computed with von Kármán's large-deflection plate equation, which is placed in nondimensional form using aerodynamic scales L and u_∞ (see Ref. 19) $(0 < x < 1)$:

$$\frac{\mu}{\lambda}\frac{\partial^4 w}{\partial x^4} - N_x\frac{\partial^2 w}{\partial x^2} + \frac{\partial^2 w}{\partial t^2} = \mu\left(\frac{1}{\gamma M_\infty^2} - p\right) \tag{1}$$

$$N_x \equiv \frac{6\mu}{\lambda}\left(\frac{h}{L}\right)^{-2}(1-\nu^2)\int_0^1 \left(\frac{\partial w}{\partial x}\right)^2 \mathrm{d}x \tag{2}$$

Aerodynamic scales were adopted for use in the development of Eqs. (1) and (2) for consistency with the preexisting flow solver used for this study (described next). The nonlinear, in-plane load in Eq. (2), serves to limit panel deflections $w(x,t)$ induced by fluid–structure interaction. The load is assumed to be distributed uniformally over the panel.[17] Equation (1) is comparable to similar formulations found in the literature,[17] although the dimensional values of w and t (denoted w_d and t_d) are scaled by h and $(\rho_s h L^4)^{1/2}$, respectively, where ρ_s is the structural density. Two pinned boundary conditions are enforced at the panel's endpoints: $w = 0$ and $\partial^2 w/\partial x^2 = 0$.

A modal solution for the deflection $w(x,t)$ is assumed:

$$w(x,t) = \sum_{i=1}^{m_s} a_i(t)\sin(i\pi x) \tag{3}$$

where m_s is the number of structural modes retained, and the modal amplitudes a_i vary in time and are collocated in the array $\boldsymbol{a}$. The Galerkin method is used to obtain a low-order set of ODEs describing the behavior of a_i (see Ref. 17). First, Eq. (3) is substituted into Eq. (1). The resulting expression is then integrated, following premultiplication by $\sin(i\pi x)$, to yield $i = 1, \ldots, m_s$:

$$\tfrac{1}{2}\ddot{a}_i + [\mu(i\pi)^4/2\lambda]a_i + (6\mu/\lambda)(h/L)^{-2}(1-\nu^2)\alpha[(i\pi)^2/2]a_i = \mu P_i \tag{4}$$

where

$$\alpha \equiv \sum_r a_r^2 \frac{(r\pi)^2}{2}$$

$$P_i \equiv \int_0^1 \left(\frac{1}{\gamma M_\infty^2} - p\right)\sin(i\pi x)\,\mathrm{d}x \tag{5}$$

The projected pressure components P_i are integrated from the aerodynamic solution with the midpoint rule, by the use of flowfield pressures on the panel surface. To accomplish the spatial integration, the panel is divided into 101 evenly spaced grid points. Although equivalent to other formulations in the literature, Eq. (4) has two notable distinctions. First, the different form of scaling described alters equation coefficients. Second, an expression relating p to the state of the panel is not assumed.[12]

The structural dynamics equation (4) is placed in first-order form by the introduction of a mode speed array $\boldsymbol{b}$, such that $\dot{a}_i = b_i$,

$$\dot{b}_i = -[\mu(i\pi)^4/\lambda + (6\mu/\lambda)(Li\pi/h)^2(1-\nu^2)\alpha]a_i + 2\mu P_i \tag{6}$$

The mode speeds and amplitudes are collocated into a structural solution array $\boldsymbol{Y}_s$, leading to a general form of the structural equation

$$\boldsymbol{Y}_s = [\boldsymbol{b}, \boldsymbol{a}]^T \tag{7a}$$

$$\dot{\boldsymbol{Y}}_s = R_s(\boldsymbol{Y}_s, \boldsymbol{P}; \mu, \lambda, h/L, M_\infty) \tag{7b}$$

For the results that follow, μ and h/L were fixed at 0.1 and 0.002, respectively, and λ was varied as a parameter.

Fluid Dynamics

The dynamics of inviscid fluid flows are governed by the Euler equations. The two-dimensional Euler equations are given hereafter in strong conservation form[20]:

$$\frac{\partial U}{\partial t} + \frac{\partial E(U)}{\partial x} + \frac{\partial F(U)}{\partial y} = 0 \tag{8a}$$

$$U(\boldsymbol{x}, t) = \begin{bmatrix} \rho \\ m_x \\ m_y \\ E_T \end{bmatrix} \tag{8b}$$

Because we assume an ideal gas for our applications, this equation set can be closed with the ideal gas law.

The solution of the Euler equations can be approximated by the use of either finite difference, finite volume, or finite element techniques. To do this approximation, the spatial domain is discretized, and the flow variables at each discrete location are collocated into a column vector $\boldsymbol{U}(t)$. Time integration across the computational mesh is used to obtain flow solutions.

Because the Euler equations are linear in the time derivative and quasi linear in the spatial derivative,[20,21] the spatial derivatives and the time derivatives in Eq. (8a) can be separated to form an evolutionary system. The evolutionary system groups the spatial derivatives of the flux terms $\partial E/\partial x$ and $\partial F/\partial y$ to form a nonlinear operator R acting on the set of fluid variables. The fluid dynamics from Eq. (8a), once discretized, can then be expressed as

$$\frac{\mathrm{d}\boldsymbol{U}(t)}{\mathrm{d}t} = R[\boldsymbol{U}(t)] \tag{9}$$

Equation (9) is referred to as the full-system dynamics. Equation (9) was solved by the use of a cell centered, finite volume scheme with second-order spatial accuracy.[20]

Time Integration of the Coupled Full-Order Equations

The systems of discretized fluid dynamic equations $\boldsymbol{U}(t)$ and modal structural equations $\boldsymbol{Y}_s$ are combined into a single time-dependent system representative of the complete interaction between structure and inviscid flow. Time integration proceeds in two steps, given an $\mathcal{O}(\Delta t)$ lag in the synchronization of fluid and structure. First, the structural variables are updated from time level n to $n+1$ with a Crank–Nicolson procedure (but limited here to only structural variables). During this step, the pressures known at grid points on the panel surface are considered frozen. In the second step, the aerodynamic variables are explicitly updated by the use of only structural variables defined at time level n.

Grid Generation and Time Step

The flow is simulated over a physical domain of length D_L, height D_H, and centered about $x = 0$. The domain is discretized by the use of $I = 141$ nodes in the streamwise direction and $J = 116$ nodes normal to the panel. Grid points are clustered in the direction normal to the panel at the panel surface, with minimum spacing denoted by $\Delta_{\text{wall}} = 0.0125$. The spacing of grid points is specified to grow geometrically from the panel boundary. In the streamwise direction, the node spacing is chosen to be uniform over the deforming panel segment, while growing geometrically upstream of the leading edge. This particular grid was shown to be converged for this flow problem with a comparable fluid solver.[12] The time step for time-accurate integration of the full-order system was the largest time increment dictiated by the stability of the fluid solver. The model problem and grid are shown in Fig. 1.

ROM Formulation

This section introduces POD and overviews Volterra methods. In addition, we fully develop the Volterra–POD approach and the synthesis of aeroelastic ROMs.

POD

POD is a technique used to identify a small number of basis functions that adequately describe the behavior of the full-system dynamics [Eq. (9)] across some parameter space of interest. A summary of POD as it applies to a spatially discretized flowfield follows. A detailed description of POD is available in the literature.[4,8]

A POD reduced-order mapping Φ is constructed by the collection of observations of the solution $\boldsymbol{U}(t) - \boldsymbol{U}_0$ at different time intervals throughout the time integration of the full-system dynamics. These observations are called snapshots[18] and are generally collected to provide a good variety of flowfield dynamics while minimizing linear dependence. The snapshot generation procedure is sometimes referred to as POD training.[8] Snapshots are compiled columnwise into a snapshot matrix S. Next, the eigenvectors V are obtained from $S^T S$. S and V produce a linear transformation Φ between the full-order solution $\boldsymbol{U}$ and the reduced-order solution $\hat{\boldsymbol{U}}$:

$$\boldsymbol{U}(t) \approx \boldsymbol{U}_0 + \Phi\hat{\boldsymbol{U}}(t) \tag{10a}$$

$$\Phi = SV \tag{10b}$$

The reduced-order variable $\hat{\boldsymbol{U}}(t)$ represents deviations of $\boldsymbol{U}(t)$ from a base solution $\boldsymbol{U}_0$. The subtraction of $\boldsymbol{U}_0$ will result in zero-valued boundaries for the POD modes wherever constant boundary conditions occur on the domain.

The reduced-order mappings for each fluid variable are developed separately, and individual S and V arrays are collocated as blocks into a larger set of arrays, also denoted S and V.

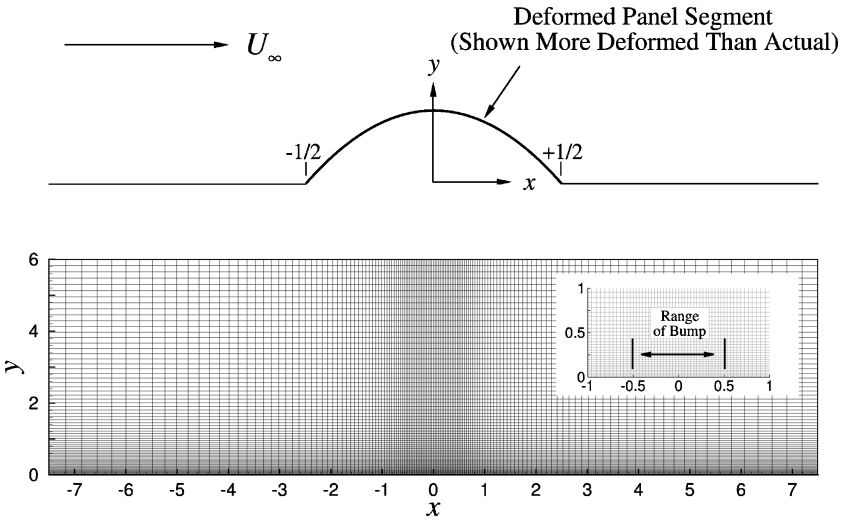

Fig. 1 Schematic of panel and coordinate system (top) and baseline grid (bottom).

POD of the discrete, panel position vector $w(x,t) \to \boldsymbol{w}(t)$ and panel velocity vector $\boldsymbol{s}(t) = \dot{\boldsymbol{w}}(t)$ are accomplished in a similar manner as that described for the fluid system. Unlike the fluid POD basis functions, there is no base term subtracted from the snapshots when a structural POD basis is generated.

Subspace projection[8] is a popular method to obtain nonlinear ROMs once the POD mapping Φ is known. Because the POD modes are orthonormal, the left inverse of Φ is simply Φ^T, and the following subspace projection ROM can be obtained from Eqs. (9) and (10a):

$$\frac{\mathrm{d}\hat{\boldsymbol{U}}(t)}{\mathrm{d}t} = \Phi^T R[\boldsymbol{U}_0 + \Phi\hat{\boldsymbol{U}}(t)] \tag{11}$$

The drawback of this approach is the computational expense of the use of the full-order operator R to time integrate the ROM.

Volterra Methods

Consider time-invariant, nonlinear, continuous-time systems. Of interest is the response of the system about an initial state $\boldsymbol{X}(0)$ due to an arbitrary input $u(t)$ for $t \geq 0$. (We take u as a real, scalar input.) As applied to these systems, Volterra theory[1,22–24] yields the response

$$\begin{aligned}\boldsymbol{X}(t) = \boldsymbol{h}_0 &+ \int_0^t \boldsymbol{h}_1(t-\tau)u(\tau)\,\mathrm{d}\tau \\ &+ \int_0^t\int_0^t \boldsymbol{h}_2(t-\tau_1, t-\tau_2)u(\tau_1)u(\tau_2)\,\mathrm{d}\tau_1\,\mathrm{d}\tau_2 \\ &+ \sum_{n=3}^{N}\int_0^t,\ldots,\int_0^t \boldsymbol{h}_n(t-\tau_1,\ldots,t-\tau_n)u(\tau_1), \\ &\ldots, u(\tau_n)\mathrm{d}\tau_1,\ldots,\mathrm{d}\tau_n\end{aligned} \tag{12}$$

Here, the Volterra kernel function is denoted $\boldsymbol{h}$.

Time is discretized with a set of time steps of equivalent size. Time levels are indexed from 0 (time 0) to n (time t), and the evaluation of $\boldsymbol{X}$ at time level n is denoted by $\boldsymbol{X}[n]$. The convolution in discrete time is

$$\begin{aligned}\boldsymbol{X}[n] = \boldsymbol{h}_0 &+ \sum_{k=0}^{N}\boldsymbol{h}_1[n-k]u[k] \\ &+ \sum_{k_1=0}^{N}\sum_{k_2=0}^{N}\boldsymbol{h}_2[n-k_1, n-k_2]u[k_1]u[k_2]\end{aligned} \tag{13}$$

Equation (13) is truncated at second order for brevity. The linearized and nonlinear Volterra kernels can be calculated directly (see Ref. 5) at considerable expense. Equation (13) can also be transformed into linearized and nonlinear (bilinear) state-space forms that can be easily implemented into other disciplines such as controls and optimization.[5,23] For linear dynamics, state-space realization with ERA has been used to generate linear, aeroelastic systems.[16] We will use ERA to synthesize aeroelastic ROMs in this paper. Nonlinear system realization remains an active area of research.

System Realization

The ERA method[15] identifies a discrete, linear, time-invariant state-space realization of the form

$$\boldsymbol{X}[n+1] = A\boldsymbol{X}[n] + B\beta\boldsymbol{u}[n] \tag{14a}$$

$$\boldsymbol{Y}[n] = C\boldsymbol{X}[n] \tag{14b}$$

by the use of data from a complete ensemble of impulse responses. The term β is a scaling parameter that is necessary to calibrate the forcing amplitude when the impulse amplitude is other than unity. Theoretically, β should be the inverse of the impulse amplitude and its inclusion allows more freedom when the full system is impulsed.

Initial state responses can be used in lieu of impulse responses, but we only consider impulse response data in this overview for simplicity. The systems realization procedure takes measurement data $\boldsymbol{Y}[n]$ from the free response of the system and produces a minimal state-space model A, B, and C such that functions $\boldsymbol{Y}$ are accurately reproduced.

The free pulse response of linear, time-invariant, discrete systems is given by a function known as the Markov parameter,

$$\boldsymbol{Y_m}[n] = CA^{n-1}B \tag{15}$$

The superposition principle states that a system response to any arbitrary input can be obtained from a linear combination of impulse responses from that system. The generalized Hankel matrix of impulse responses is related to the Markov parameter by the superposition principle. The Hankel matrix is formed by windowing the impulse response data. A total of K data points are provided at discrete time steps $n = 1,\ldots,K$, and the $r \times s$ matrix H_{rs} is formed as follows:

$$H_{rs}^{n-1} = \begin{bmatrix} \boldsymbol{Y_m}[n] & \ldots & \boldsymbol{Y_m}[n+s-1] \\ \boldsymbol{Y_m}[1+n] & \ldots & \boldsymbol{Y_m}[1+n+s-1] \\ \vdots & \vdots & \vdots \\ \boldsymbol{Y_m}[r-1+n] & \ldots & \boldsymbol{Y_m}[r-1+n+s-1] \end{bmatrix} \tag{16}$$

where s is the total size of the data window, and r is the number of time steps used to shift the data window. The choice of r and s is arbitrary as long as $r+s+n \leq K+2$.

The ERA method eliminates redundant data by the use of singular value decomposition (SVD) on H_{rs}^0,

$$H_{rs}^0 = P D Q^T \tag{17}$$

Unwanted state dimensionality is eliminated by truncation of the elements of P, D, and Q associated with very small singular values of H_{rs}^0. The number of states is reduced to a minimal number q. The number of observations p and the number of forcing terms m are known from the problem formulation. The dimension of the Markov parameter $\boldsymbol{Y_m}[n]$ is $p \times m$. Algebra is used to recast Eq. (15) in terms of the time-shifted Hankel matrix H_{rs}^1 and the elements P, D, and Q. The state-space realization flows from this manipulation and is as follows:

$$A = D^{-\frac{1}{2}} P^T H_{rs}^1 Q D^{-\frac{1}{2}} \tag{18a}$$

$$B = D^{\frac{1}{2}} Q^T E_m \tag{18b}$$

$$C = E_p^T P D^{\frac{1}{2}} \tag{18c}$$

E_p^T and E_m^T are defined as

$$E_p^T = [I_p, 0_p, \ldots, 0_p] \tag{19a}$$

$$E_m^T = [I_m, 0_m, \ldots, 0_m] \tag{19b}$$

where 0_p and 0_m are the null matrices of order p and m, respectively, and I_p and I_m are the identity matrices of order p and m.

Because the discrete time step $\Delta t = t_{k+1} - t_k$ is constant, the continuous form of the discrete state-space realization is easily obtained. The continuous from, shown hereafter, absorbs the scaling parameter β into the matrix B and may require additional state dimensionality when the discrete realization has real, negative poles:

$$\dot{\boldsymbol{X}}(t) = A\boldsymbol{X}(t) + B\boldsymbol{u}(t), \qquad \boldsymbol{Y}(t) = C\boldsymbol{X}(t) \tag{20}$$

Aeroelastic ROM Development

POD provides a transformation Φ that maps $\boldsymbol{U}(t)$ to a low-order vector of modal coefficients $\hat{\boldsymbol{U}}(t)$ [from Eq. (10a)]. The reduced-order fluid variable $\hat{\boldsymbol{U}}(t)$ will be denoted $\boldsymbol{Y}_f$, which is the vector of outputs $\boldsymbol{Y}(t)$ [Eq. (20)].

A state-space model for $\boldsymbol{Y}_f$ can be obtained from impulse responses with the ERA method. Impulses for the fluid system use the plate position and velocity coefficients ($\boldsymbol{Y}_s$) as the forcing terms. Each structural term is impulsed, and the fluid system response is generated by the use of the full-order model. The time history of the impulse response is projected onto each of the POD basis functions within Φ to obtain the impulse response of the reduced-order fluid vector $\boldsymbol{Y}_f$. POD basis functions Φ are obtained by the use of the method of snapshots as described earlier. The process is repeated for each structural mode, and the collection of impulse responses is used to generate a linear state-space model for the reduced-order fluid system

$$\dot{\boldsymbol{X}}_f = A_f \boldsymbol{X}_f + B_f \boldsymbol{Y}_s \tag{21a}$$

$$\boldsymbol{Y}_f = C_f \boldsymbol{X}_f \tag{21b}$$

where $\boldsymbol{X}_f$ is the state vector from the ROM realization and $\boldsymbol{Y}_s$ represents the modal coefficients for the structural deformation.

The structural model from Eq. (7b) is coupled to the reduced-order fluid model [Eqs. (21a) and (21b)] through the projected pressure term $\boldsymbol{P}$. The reduced-order variables $\boldsymbol{Y}_f$ are obtained from the dynamic states $\boldsymbol{X}_f$ by the linear mapping C_f. Fluid pressure on the panel is extracted from $\boldsymbol{Y}_f$ with the portion of the reduced-order mapping [Eq. (10a)] that pertains to the moving boundary. Equation (5) is used to project the pressure values into $\boldsymbol{P}$. The mapping of reduced-order fluid states to projected pressure is denoted f_P,

$$\boldsymbol{P} = f_P(\boldsymbol{X}_f) \tag{22}$$

Equation (22) is used to couple the structure and fluid dynamic state variables,

$$\dot{\boldsymbol{Y}}_s = R_s[\boldsymbol{Y}_s, f_P(\boldsymbol{X}_f); \mu, \lambda, h/L, M_\infty] \tag{23}$$

Equations (21a) and (23) comprise the low-order, aeroelastic ROM with linear fluid dynamics and nonlinear plate dynamics.

The fluid and structural terms are grouped into arrays $\boldsymbol{Y}_{\text{ae}}$ and $\hat{R}$, as follows:

$$\boldsymbol{Y}_{\text{ae}} = \begin{bmatrix} \boldsymbol{X}_f \\ \boldsymbol{Y}_s \end{bmatrix} \tag{24}$$

$$\hat{R} = \begin{bmatrix} A_f \boldsymbol{X}_f + B_f \boldsymbol{Y}_s \\ R_s[\boldsymbol{Y}_s, f_P(\boldsymbol{X}_f); \mu, \lambda, h/L, M_\infty] \end{bmatrix} \tag{25}$$

The reduced-order, aeroelastic system is denoted as simply

$$\dot{\boldsymbol{Y}}_{\text{ae}} = \hat{R}(\boldsymbol{Y}_{\text{ae}}) \tag{26}$$

Time Integration of the Aeroelastic System

The aeroelastic ROM [Eq. (26)] is integrated in time with the two-time level, second-order accurate, Crank–Nicolson method. At each time level, an updated solution is computed by the use of a chord technique with a time-frozen Jacobian that uses the base flow condition and $\boldsymbol{Y}_s = 0$. Typically, one to two subiterations are sufficient to drive iterative residuals to near machine zero. Because peak panel deflection is no more than 2% of panel length for the cases considered, the chord method is rapidly convergent.

Results

The results that follow consider supersonic freestream flow conditions at Mach 1.2 with sea-level conditions. The Galerkin panel model contains four modes for a total of eight DOF. The panel dynamic pressure λ is treated as a parameter and is varied to produce a variety of panel LCO amplitudes. At Mach 1.2, panel LCO occurs for values of $\lambda > 17$ (Refs. 10 and 12).

Impulse Response of a Supersonic Fluid

Impulsing the forcing term (or terms) of a truly linear system produces a response that is the building block necessary to recreate the system output from any arbitrary forcing function. Linear superposition allows the response of the system to be constructed in this fashion because any forcing function can be assembled from a series of impulses.

The supersonic flowfield was essentially linear[10] once LCO was fully developed. Shock waves formed at the ends of the panel, and, although they varied in strength dynamically with the LCO, they were stationary. Also, the flowfield between the shocks (directly over the panel) was linear for this case. However, impulsing the uniform, supersonic flowfield with structural modes (and modal velocities) produced very nonlinear transient behavior. Figure 2 shows density contours of the flow 1.10802 nondimensional time units from the impulse of the fundamental structural velocity mode. The sudden appearance of a velocity profile on the boundary, and its sudden removal one time step later, produced a shock wave of varying strength running the length of the panel. Early on during the transient period, this shock welled upward away from the panel and convected downstream. The convection of the shock combined with the patterns of varied intensity produce the odd (but physical) spatial oscillation above the panel shown in Fig. 2. After about 2.5 time units, this pattern had both convected well beyond the end of the panel and diffused into a more benign flow pattern. After 25 time units uniform flow was restored. The flow dynamics were essentially linear after the initial 2.5 time unit transient.

The results that follow will detail the usefulness of such impulse responses for the generation of a reduced-order fluid model. The linear portion of the impulse response time integrations contained some of the LCO flowfield characteristics, otherwise, none of the ROM options would have reproduced LCO. However, the impulse

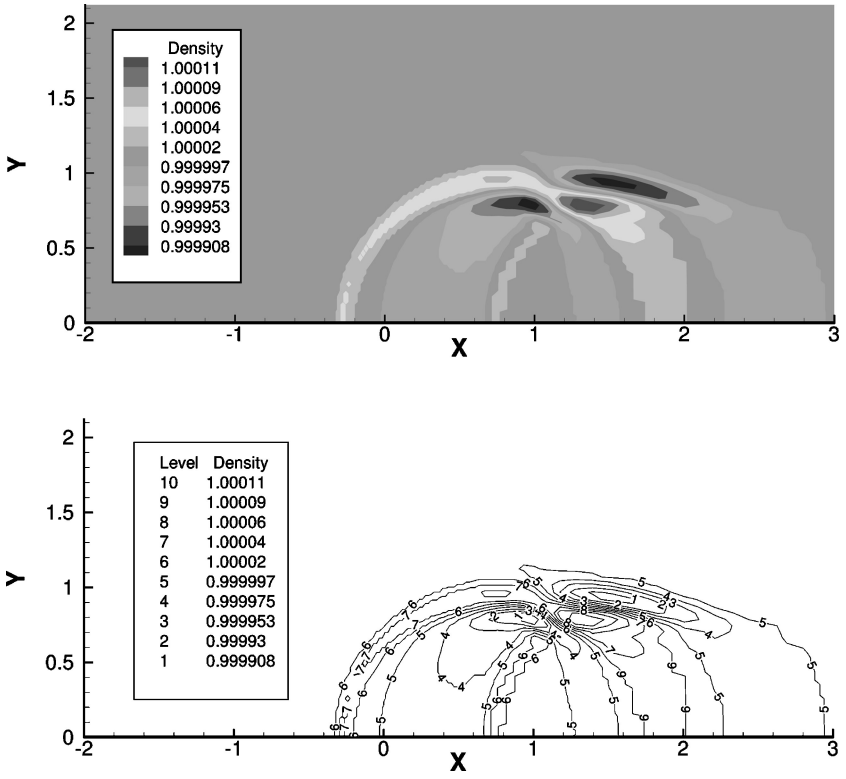

Fig. 2 Density contours 1.10802 time units after impulse.

responses themselves would not produce POD basis functions capable of correctly modeling the LCO flowfield. This outcome suggests that the supersonic flowfield was not truly linear.

Identification of Fluid Modes

Fluid modes were obtained by the use of POD as outlined earlier. Aeroelastic fluid modes were obtained from a set of 100 snapshots. Snapshots of the full-order, aeroelastic system were taken at equally spaced intervals, from startup through 25 time units, by the use of time integration of the full system, with $\lambda = 25$. For all time integration cases that follow, the aeroelastic system was initialized with the base flow condition and a small perturbation (height of 0.0001) in the fundamental panel position mode [denoted a_1 in Eq. (7a)]. Snapshots were taken of primitive fluid variables ρ, u, v, and E_T, not the conserved variables given in Eq. (8b). Primitive variables enable Galerkin projection for the fluid as a possible means for obtaining nonlinear terms in future analysis (see Ref. 14). At Mach 1.2, LCO required about 300 time units to become fully developed, and the small 25 time unit training window was shown to be adequate in previous work.[10,12]

The results that follow refer to two cases. For the first case, the base flow term $\boldsymbol{U}_0$ from Eq. (10a) consisted of uniform, freestream conditions everywhere throughout the domain (referred to as slug flow). The second case considered steady-state flow over the initial panel perturbation as the base flow term $\boldsymbol{U}_0$. The second case was included because initially it was thought that the base flow term should contain the stationary shocks at the leading and trailing edges of the panel. In this second case, the aeroelastic POD modes would model only linear flow structures over the panel and would not have to account for the formation of the leading- and trailing-edge shocks. For both cases, the first two modes for each fluid variable contained over 98% of the energy content, and system realization was performed with a total of $M = 8$ fluid modes (two modes per fluid variable). An attempt was also made to use the impulse response data as snapshots, in lieu of aeroelastic time integration. The same systems realization procedure was repeated to produce a Volterra–POD ROM for this third case, but this ROM did not correctly produce LCO. Our observations and recommendations regarding this third approach are documented in a separate section.

System Realization

Eight POD modes were considered (the dimensionality of $\boldsymbol{Y}_f$), which produced eight impulse responses for each forcing function. With eight forcing terms in $\boldsymbol{Y}_s$, the total number of impulse responses numbered 64. Realization via the ERA process for each of the aeroelastic cases is detailed hereafter.

Uniform Base Flow

A state-space realization of the form in Eqs. (14a) and (14b) was obtained by the use of ERA for the slug-flow base case. The impulse amplitude was chosen arbitrarily to be 0.1. The full-system response to this impulse was sampled over 30 nondimensional time units at a rate of $\mathrm{d}t = 0.015432$ for a total of $K = 1944$ discrete data points. The fluid system impulse response was generated with the full-order model. The time history of the full-order impulse response was projected onto each of the POD basis functions to obtain the impulse response of the reduced-order fluid variable $\boldsymbol{Y}_f$. The data were windowed with $s = 192$ and $r = 100$. Every fifth data point was used in the realization algorithm, providing data at the rate of $\mathrm{d}t = 0.07716$. These values of $\mathrm{d}t$, s, and r were chosen by trial and error to produce realizations whose impulse responses closely matched the data. The value of m was eight to match the number of forcing terms, and $p = 8$ was chosen to match the number of ROM coefficients. The collection of impulse responses formed an 8×8 Markov parameter $\boldsymbol{Y}_m[n]$ function from Eq. (15). The number of states, $q = 8$, was chosen to match the number of ROM coefficients, so that SVD on the Hankel matrix formed from $\boldsymbol{Y}[n = 1]$ was used to truncate all but the largest eight singular values, yielding the matrices P, D, and Q. Equations (18a–18c) were then used to generate a linear state-space model for the reduced-order fluid system.

The value of the scaling parameter in Eq. 14a was $\beta = 650$. This value was determined when the ROM results were tuned to the snapshot data. Theoretically, β should have been the inverse of the impulse size ($\beta = 1/0.1 = 10$). The need for an order magnitude increase in β reveals an inefficiency in projecting the impulsed flowfield onto the aeroelastic modes in Φ. Evidently, the impulsed flowfield contained structures not adequately represented in Φ, and a significant amount of flow energy was not captured in the

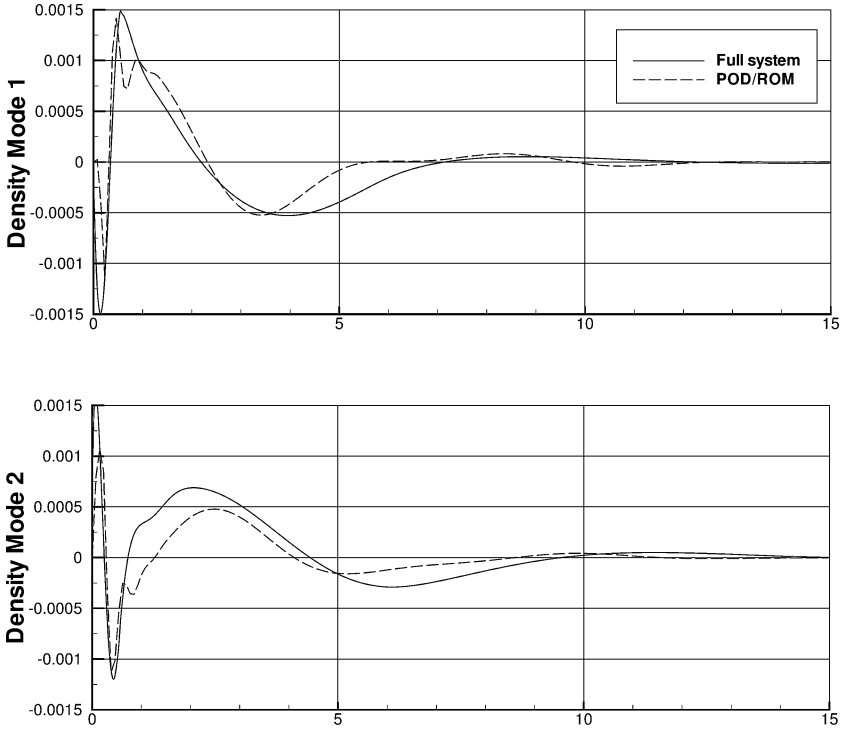

Fig. 3 Response of density modes to velocity term impulse, uniform base flow case.

projections used to compute the modal-impulse behavior. However, enough linear, aeroelastic information was resident in the impulsed flowfield for the Volterra–POD realization to produce correct results (with β properly adjusted).

The impulse response of Eqs. (14a) and (14b) was obtained with $\beta = 1$. The impulse responses of the reduced-order system were in good agreement with the impulse responses from the full-order system used by ERA. The response of the two density modes to an impulse in the first panel velocity term b_1 within $\boldsymbol{Y}_s$ [defined in Eq. (7a)] are shown in Fig. 3. The continuous form of Eqs. (14a) and (14b) were obtained via a function call in MATLAB®, which provided the matrices A_f, B_f, and C_f for time integration of the aeroelastic model given in Eq. (26).

Steady-State Base Flow

The same procedure was repeated, but the aeroelastic modes were computed with a steady-state base flow condition described earlier. For this realization, every 20th data point was used in the realization algorithm, providing data at the rate of $\mathrm{d}t = 0.3086$. The same impulse amplitude of 0.1 was used for this case, and the full-system impulse response was sampled at the same rate. However, the impulses were added to the steady-state panel deflection for this case. The data were windowed by the use of $s = 47$ and $r = 20$. The scaling parameter from Eq. (14a) was $\beta = 800$ and was determined when the ROM was tuned to the snapshot data. The larger value of $\mathrm{d}t$ eliminated much of the high-frequency transient and focused ERA on the low-frequency portion of the impulse response.

ROM Time History

Both the slug-flow base case and the steady-state base case Volterra–POD ROMs, described earlier, were time-integrated with the aeroelastic training conditions of Mach 1.2 and $\lambda = 25$. The results are shown in Fig. 4. Both cases correctly predicted LCO, but the steady-state base case was more accurate in amplitude, frequency, and phase than the slug-flow base case. The three-quarter chord panel amplitude was muted by 9% for the steady-state base case and magnified by 25% for the slug-flow base case. The phase and frequency error were negligible for the steady-state base case, but the larger amplitudes of the slug-flow base case introduced a small increase in LCO frequency (resulting in an accumulating phase error).

The improvement in performance associated with the steady-state base flow was most likely due to the choice of data windowing parameters used in the ERA realization. There was no substantive differences in either the POD modes or the impulse response of the full-system flowfield. The original concern that shocks needed to be present in the base flow term was not an issue. Shocklike structures were present in both base flow cases. Data windowing parameters were selected to provide a realization whose impulse response closely matched the original impulse data. As noted earlier, reducing the size of $\mathrm{d}t$ introduced high-frequency dynamics into the realization. The slug-flow base case was formed by the use of a very small value of $\mathrm{d}t$. Consequently, the impulse response of the model (Fig. 3) matched the initial transient in the data better than the steady-state base flow case, which used a much larger $\mathrm{d}t$. However, the high-frequency data in the impulse response were not germane to the large-time behavior of the aeroelastic system, and its inclusion resulted in a less accurate ROM under aeroelastic conditions.

ROM Robustness

Both aeroelastic ROMs were time-integrated with a variety of panel dynamic pressure values λ. The intent was to explore the predictive accuracy of the Volterra–POD ROMs across a nonlinear parameter space. Both ROMs were trained at $\lambda = 25$ (as described earlier), and robustness was defined as the ROM's ability to predict panel amplitude (at the three-quarter chord position) in fully developed LCO across the parameter space, including non-LCO cases.

The ROM results are compared with full system results and results from the literature[25] in Fig. 5. The steady-state base case ROM was better suited to large LCO amplitudes. Larger panel amplitudes excited a panel nonlinearity that, in turn, excited a high-frequency response from the slug-flow base case. As discussed earlier, the high-frequency content in the slug-flow based ROM was not germane to the LCO flowfield and corrupted the results at large LCO amplitudes. Conversely, the use of slug flow as the base flow term permitted a more accurate prediction of LCO onset at the lower values of λ. A non-LCO solution for the slug-flow base case occurred when both the fluid and structural modal coefficients were zero valued

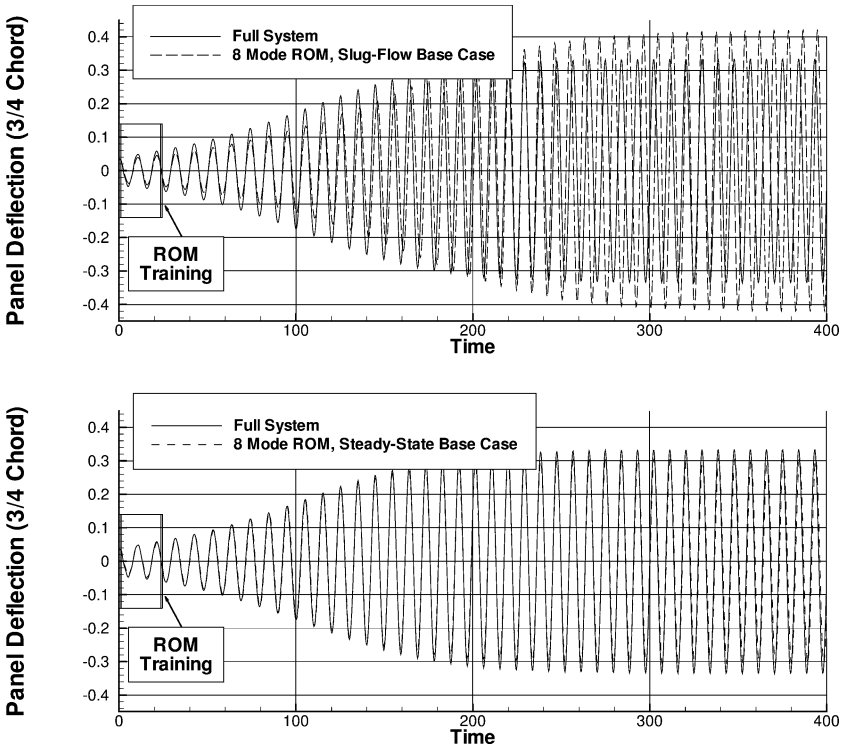

Fig. 4 Panel deflection (w_d/h) time history, $\lambda = 25$, Mach 1.2.

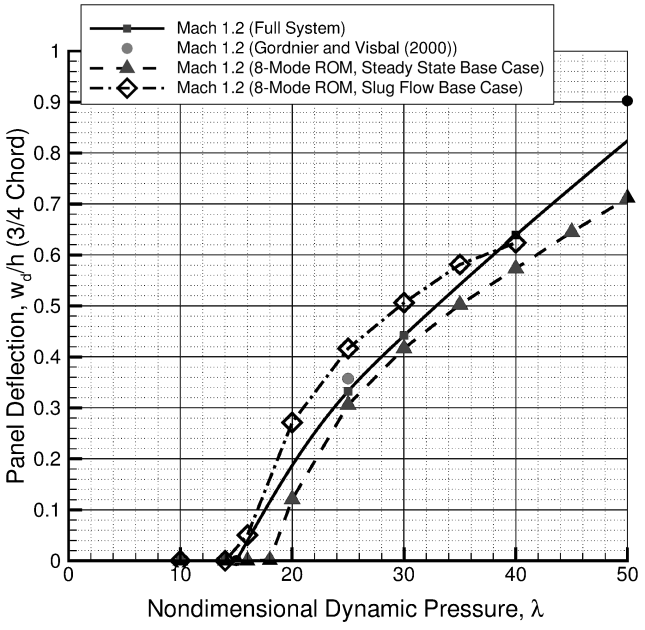

Fig. 5 Panel response vs dynamic pressure.

($\boldsymbol{Y}_f = [0]$ and $\boldsymbol{Y}_s = [0]$). In addition, the small panel amplitudes near LCO onset did not excite the high-frequency errors in the slug-flow base case that were evident at larger values of λ. In comparison, the stead-state based ROM had difficulty producing the zero panel deflection state $\boldsymbol{Y}_s = [0]$ because this panel condition required slug flow. Slug-flow conditions were not well represented in the ROM training, and the value of the fluid modal coefficients $\boldsymbol{Y}_f$ to produce slug flow was not easily obtained in the time integrations.

Aeroelastic Structural Modes

Aeroelastic structural modes were generated by the use of 100 snapshots of the structural response obtained during the training of the fluid ROM. The structural snapshots corresponded exactly in time with the set of 100 snapshots used to construct the fluid ROMs. Snapshots were taken of the panel position and velocity vectors [$\boldsymbol{w}(t)$ and $\dot{\boldsymbol{w}}(t)$, respectively], and subspace projection[8] was used to form a nonlinear, reduced-order structural model. [See Eq. (11).] Subspace projection relied on the Galerkin panel model for time integration. The panel position and velocity from the Galerkin panel model were projected onto the POD basis functions at every step in the time integration. Subspace projection demonstrated the adequacy of the POD modes at capturing the dynamic panel behavior while maintaining the nonlinearity of the panel dynamics.

The reduced-order structural model was tightly coupled with the steady-state base case fluid ROM and time-integrated with the parameter value $\lambda = 25$. Figure 6 compares the results with the full-system response and the POD/ROM results from Fig. 4 (for the steady-state base case). For clarity, the top, right-hand corner of the entire time response is expanded in the lower portion of Fig. 6. Two POD modes per structural variable (four DOF total) yielded essentially identical results to the four mode (eight DOF) Galerkin result. Further order reduction greatly decreased the panel response. For this problem, the full-system structural model was very low order, and the additional order reduction from POD was immaterial. However, future application of this technique will involve very high-order, nonlinear structural models requiring order reduction along with the fluid model. These results demonstrate that a single training event can produce adequate POD modes for both the fluid and structure.

ROMs Using Impulse Response Modes

As an excursion, the aeroelastic fluid modes were replaced with POD modes derived from the impulse responses of the full system. There were 40 snapshots collected from each of the eight impulse responses generated when the elements of $\boldsymbol{Y}_s$ were impulsed. The snapshots were taken at even intervals over a time integration lasting 30 time units. Because there were eight impulse responses, a total of 320 snapshots were generated. Over 98% of the flow energy was contained in the first four modes for each of the four fluid variables. This suggests that a 16-mode ROM would be adequate for the fluid. To test the adequacy of the POD basis, the full-system flow solution from time integration with $\lambda = 25$ and Mach 1.2 was

projected onto the POD basis during time integration. The modal amplitudes were examined, and modes 6–8 in energy content had a much greater contribution to the aeroelastic flowfield than did the first four modes. (Note that the modes were normalized.) This observation motivated the use of 10 modes per fluid variable for ROM realization. ERA was used to synthesize a 40-mode ROM, which required 43 states after conversion to the continuous form. The Volterra–POD ROM was coupled with the Galerkin panel model as described earlier.

Unfortunately, the aeroelastic ROM produced a slowly divergent flutter instead of LCO. However, the panel pressures from the Volterra–POD ROM corresponded very well with the pressures obtained by the projection of the full-system response onto the POD basis and extraction of the panel pressures (Fig. 7). This result further suggests that the POD basis derived from the impulse response data was not adequate for modeling the aeroelastic flowfield. The accuracy of the ROM at representing the full-system response was encouraging, and the frequency of unstable oscillations matched the LCO frequency. Some flowfield structure in the impulse response modes is relevant to LCO, but more investigation is required before these modes can be used to generate an accurate ROM for the supersonic case.

Computational Performance

The motivation for employment of the POD–Volterra approach was to realize a computational performance improvement consistent with the reduction in the number of DOF. Computational performance, given in Table 1, was assessed by measurement of the wall clock time to provide fully developed LCO of the flow (400 time units with $\lambda = 25$). All computations were run on a 800-MHz Pentium-based personal computer. The full-system, non-Galerkin ROM, and POD–Volterra solvers were written in FORTRAN by a single programmer. The compiler options and I/O requirements were chosen to provide the quickest run times, and these settings were identical for the full-system and reduced-order solvers.

Table 1 Computational performance

Flow solver	Fluid DOF	Wall clock time, s
Full-order	64,400	22,304
POD–Volterra	8	8.132

The time step used for the full system was based on a Courant–Friedrichs–Lewy condition of 0.5, which was the highest value allowing for stability of the second-order method. The reduced-order time integration used a time step size of 0.05 time units. The POD–Volterra ROM reduced compute time by four orders of magnitude and realized an improvement in performance consistent with the DOF reduction.

The cost of computing the state-space realization with ERA was small relative to the cost of a full-system analysis. Because there were eight forcing terms, eight additional runs of the full-order solver were required to provide the impulse response data. Each 25 time unit impulse response run required 1394 s wall-clock time, resulting in 11152 s of computer time for generation of the impulse response data. An additional 25 time unit run was required for snapshot collection to generate the aeroelastic modes, bringing the total computer processing time to 12546 s, roughly one-half of the computational cost associated with a single full-system time integration.

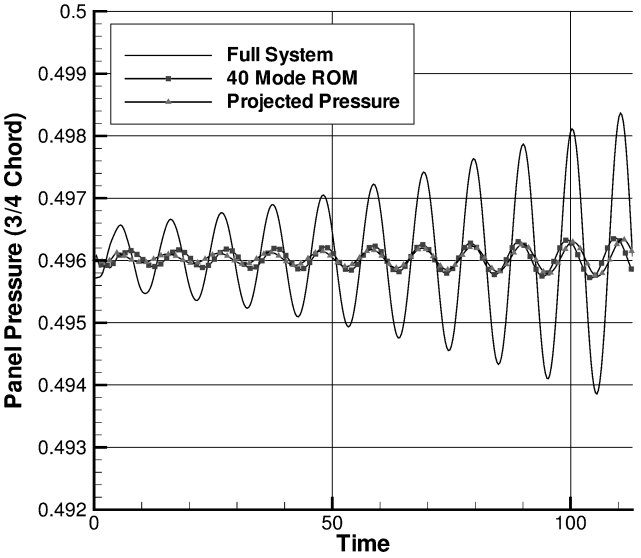

Fig. 7 Panel pressure degradation by the use of impulse response modes.

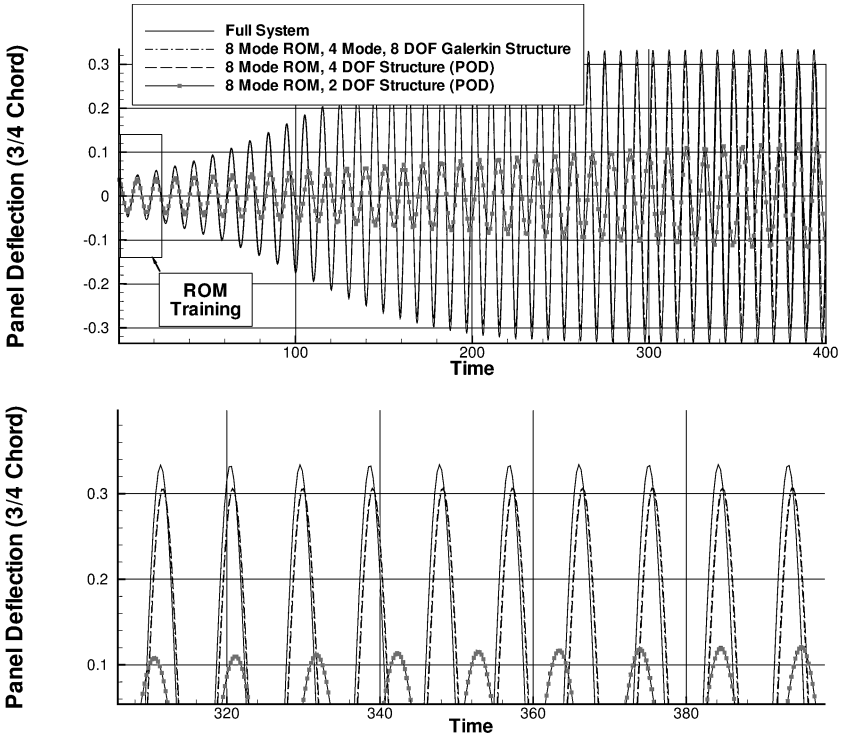

Fig. 6 Panel response (w_d/h) with aeroelastic structural modes.

Conclusions

The Volterra–POD approach produced a stable and accurate aeroelastic ROM with four orders of magnitude reduction in problem order and computational expense. Aeroelastic modes were formed from snapshots obtained during the initial buildup of LCO with a fixed value of dynamic panel pressure. The full-system model was impulsed with the structural velocity and position modes. The flowfield was projected onto the aeroelastic modes to determine the modal amplitudes, and a linear, state-space realization for the fluid dynamics was synthesized from the modal impulse responses. The fluid and structural models were tightly coupled to form the aeroelastic ROM. Two cases were considered. The first case used uniform flow as a base term about which perturbations were computed by the reduced-order fluid model. The second case used steady-state flow over the initial panel deflection as the base flow term. Both cases resulted in ROMs that correctly predicted LCO behavior over a wide parameter space; however, the uniform base flow was more desirable for the prediction of LCO onset. In addition, it was desirable to filter high-frequency information out of the impulse response data by computation of the realization with relatively large time steps.

Fluid modes obtained from snapshots of the impulsed flowfield were found to be inadequate for accurate reduced-order modeling of the supersonic, aeroelastic flowfield. However, only an initial attempt was made to examine this approach, and additional research should be conducted before the technique is dismissed completely.

Reduced-order modeling of the structure was also explored, and the results demonstrated that a single training event could produce adequate POD modes for both the fluid and structure. Future applications of this technique will involve very high-order, nonlinear structural models requiring order reduction along with the fluid model.

Acknowledgment

The authors gratefully acknowledge the support of the U.S. Air Force Office of Scientific Research under Grant 99VA01COR (Dean T. Mook, Program Manager).

References

[1]Volterra, V., *Theory of Functionals and of Integral and Integro-Differential Equations*, Dover, New York, 1959.

[2]Loeve, M., *Functions Aleatoire de Second Ordre*, C. R. Academie des Sciences, Paris, 1945.

[3]Karhunen, K., *Zur Spektral Theorie Stochastischer Prozesse*, Ann. Acad. Sci. Fennicae, Ser, 1946.

[4]Berkooz, G., Holmes, P., and Lumley, J. L., "The Proper Orthogonal Decomposition in the Analysis of Turbulent Flows," *Annual Reviews of Fluid Mechanics*, Vol. 25, 1993, pp. 539–575.

[5]Silva, W. A., "Discrete-Time Linear and Nonlinear Aerodynamic Impulse Responses for Efficient CFD Analyses," Ph.D. Dissertation, College of William and Mary, Williamsburg, VA, Dec. 1997.

[6]Silva, W. A., "Reduced-Order Models Based on Linear and Nonlinear Aerodynamic Impulse Responses," *CEAS/AIAA/ICASE/NASA Langley International Forum on Aeroelasticity and Structural Dynamics*, 1999, pp. 369–379.

[7]Raveh, D., Levy, Y., and Karpel, M., "Aircraft Aeroelastic Analysis and Design Using CFD-Based Unsteady Loads," AIAA Paper 2000-1325, April 2000.

[8]Beran, P. S., and Pettit, C. L., "Prediction of Nonlinear Panel Response Using Proper Orthogonal Decomposition," AIAA Paper 2001-1292, April 2001.

[9]Pettit, C. L., and Beran, P. S., "Reduced-Order Modeling for Flutter Prediction," *41st AIAA/ASCE/AHS/ASC Structures, Structural Dynamics and Materials Conference*, AIAA, Reston, VA, 2000; also AIAA Paper 2000-1446-CP, 2000.

[10]Beran, P., and Silva, W., "Reduced-Order Modeling: New Approaches for Computational Physics," AIAA Paper 2001-0853, Jan. 2001; also in Progress in Aerospace Sciences, Vol. 40, pp. 51–177.

[11]Lucia, D. J., Beran, P. S., and King, P. I., "Reduced Order Modeling of an Elastic Panel in Transonic Flow," *Journal of Aircraft*, Vol. 40, No. 2, 2003, pp. 338–347.

[12]Beran, P. S., Lucia, D. J., and Pettit, C. L., "Reduced Order Modeling of Limit-Cycle Oscillation for Aeroelastic Systems," IMECE Paper 2002-32954, Nov. 2002.

[13]Lucia, D. J., and Beran, P. S., "Projection Methods for Reduced Order Models of Compressible Flows," *Journal of Computational Physics*, Vol. 188, No. 1, 2003, pp. 252–280.

[14]Lucia, D. J., and Beran, P. S., "Reduced Order Model Development Using Proper Orthogonal Decomposition and Volterra Theory," *AIAA Journal* (to be published).

[15]Juang, J. N., and Pappa, R. S., "An Eigensystem Realization Algorithm for Modal Parameter Identification and Model Reduction," *Journal of Guidance, Control, and Dynamics*, Vol. 8, No. 5, 1984, pp. 620–627.

[16]Silva, W. A., and Bartels, R. E., "Development of Reduced Order Models for Aeroelastic Analysis and Flutter Prediction Using the CFL3Dv6.0 Code," AIAA Paper 2002-1594, April 2002.

[17]Dowell, E. H., "Nonlinear Oscillations of a Fluttering Plate," AIAA Journal, Vol. 4, No. 7, 1966, pp. 1267–1275.

[18]Sirovich, L., "Turbulence and the Dynamics of Coherent Structures. Part I: Coherent Structures," *Quarterly of Applied Mathematics*, Vol. 45, No. 3, 1987, pp. 561–571.

[19]Selvam, R. P., and Morton, S. A., "Computation of Nonlinear Viscous Panel Flutter," AIAA Paper 1844, April 1998.

[20]Tannehill, J. C., Anderson, D. A., and Pletcher, R. H., *Computational Fluid Mechanics and Heat Transfer*, 2nd. ed. Hemisphere, Washington, DC, 1997.

[21]Stakgold, I., Green's *Functions and Boundary Value Problems*, 2nd ed., Wiley, Washington DC, 2nd ed., 1998.

[22]Schetzen, M., *The Volterra and Wiener Theories of Nonlinear Systems*, Wiley, New York, 1980.

[23]Rugh, W. J., *Nonlinear System Theory, The Volterra-Wiener Approach*, John Hopkins Univ. Press, Baltimore, MD, 1981.

[24]Bendat, J. S., *Nonlinear System Analysis & Identification from Random Data*, Wiley-Interscience, New York, 1990.

[25]Gordnier, R. E., and Visbal, M. R., "Development of a Three-Dimensional Viscous Aeroelastic Solver for Nonlinear Panel Flutter," AIAA Paper 2000-2337, June 2000.